Molecular basis underlying histone H3 lysine–arginine methylation pattern readout by Spin/Ssty repeats of Spindlin1

Xiaonan Su,[1,2,6] Guixin Zhu,[1,3,6] Xiaozhe Ding,[1,2] Shirley Y. Lee,[4] Yali Dou,[4] Bing Zhu,[5] Wei Wu,[1,7] and Haitao Li[1,2,7]

[1]Ministry of Education Key Laboratory of Protein Sciences, School of Life Sciences, Tsinghua University, Beijing 100084, China; [2]Center for Structural Biology, Department of Basic Medical Sciences, School of Medicine, Tsinghua University, Beijing 100084, China; [3]Tsinghua-Peking Center for Life Sciences, Beijing 100084, China; [4]Department of Pathology, University of Michigan, Ann Arbor, Michigan 48109, USA; [5]National Institute of Biological Sciences, Beijing 102206, China

Histone modification patterns and their combinatorial readout have emerged as a fundamental mechanism for epigenetic regulation. Here we characterized Spindlin1 as a histone effector that senses a *cis*-tail histone H3 methylation pattern involving trimethyllysine 4 (H3K4me3) and asymmetric dimethylarginine 8 (H3R8me2a) marks. Spindlin1 consists of triple tudor-like Spin/Ssty repeats. Cocrystal structure determination established concurrent recognition of H3K4me3 and H3R8me2a by Spin/Ssty repeats 2 and 1, respectively. Both H3K4me3 and H3R8me2a are recognized using an "insertion cavity" recognition mode, contributing to a methylation state-specific layer of regulation. In vivo functional studies suggest that Spindlin1 activates Wnt/β-catenin signaling downstream from protein arginine methyltransferase 2 (PRMT2) and the MLL complex, which together are capable of generating a specific H3 "K4me3–R8me2a" pattern. Mutagenesis of Spindlin1 reader pockets impairs activation of Wnt target genes. Taken together, our work connects a histone "lysine–arginine" methylation pattern readout by Spindlin1-to-Wnt signaling at the transcriptional level.

Histone post-translational modifications (PTMs) have been proposed to constitute a "histone code," which helps to organize genetic information at the chromatin level, and play an important role in gene expression, cell differentiation, and development (Jenuwein and Allis 2001). More than 200 distinct histone PTMs have been identified to date. It has been proposed that histone PTMs act as binding sites or marks for recruitment of downstream effectors. During the past decade, a wealth of "reader" modules have been characterized for histone PTM recognition that function in a histone type- and site-specific manner. Examples of such modules include Bromo, Chromo, Tudor, MBT, PWWP, WD40, PHD finger, CW finger, and BAH domains (Taverna et al. 2007; Musselman et al. 2012; Patel and Wang 2013). Intriguingly, recent progress suggests that the "ON" and "OFF" states of chromatin are not simply determined by a single histone mark readout, but rather, histone PTMs often exist as patterns that can be recognized by paired reader modules to bring out particular functional outcomes (Ruthenburg et al. 2007; Wang and Patel 2011).

Histone methylation marks are among the most extensively studied histone PTMs and have been implicated in multiple cellular processes (Greer and Shi 2012). Both lysine and arginine residues of histones can be methylated by a diverse family of histone lysine methyltransferases (KMTs) or protein arginine methyltransferases (PRMTs). Histone lysines can be monomethylated (Kme1), dimethylated (Kme2), and trimethylated (Kme3) by KMTs in a site- and state-specific manner. The molecular basis for site- and state-specific readout of histone methyllysine marks by reader modules has been well established (Taverna et al. 2007). Arginine methylation also exists in three states— monomethylation (Rme1), asymmetrical dimethylation

(Rme2a), and symmetrical dimethylation (Rme2s)—catalyzed by type I (for Rme1 and Rme2a) or type II (Rme1 and Rme2s) PRMTs (Yang and Bedford 2013). Methylation of histone arginine sites has been well characterized in histone H3 at positions R2, R8, R17, and R26; histone H4 at position R3; histone H2A at positions R3 and R29; and so forth (Di Lorenzo and Bedford 2011). However, only a few effectors have been described for recognition of histone arginine methylation marks (Chen et al. 2011; Patel and Wang 2013), whose molecular basis was recently revealed for histone H3R2me2s readout by WD40 repeats of WDR5 (Migliori et al. 2012) and implicated in RNA polymerase II CTD Rme2a readout by the TDRD3 Tudor domain (Yang et al. 2010; Liu et al. 2012; Sikorsky et al. 2012). Additional cases for site- and state-specific histone arginine methylation readout remain to be elucidated in molecular detail. Besides, adjacent histone arginine and lysine methylation marks have been shown to coexist as a pattern of dual marks, such as H3 R2me2a–K4me3, R8me2s–K9me3, and R26me2a–K27me3 (Migliori et al. 2010; Di Lorenzo and Bedford 2011). In most cases, such patterns were reported to be involved in "binary switch" control, in which two neighboring methyl marks negatively affect each other, thereby impeding either effector binding or enzymatic modification (Migliori et al. 2010). Hence, it remains an open question whether a histone "lysine–arginine" methylation pattern does exist that can function through combinatorial readout and exhibit cooperatively.

Spindlin1, a member of the Spin/Ssty family of proteins, which are highly conserved in vertebrates (Staub et al. 2002), was initially identified as an abundant maternal factor in mouse oocyte and early embryo formation (Oh et al. 1997). Spindlin1 localizes to cell nuclei and displays spindle as well as chromatin-binding activity during meiosis or mitosis (Oh et al. 1997; Yuan et al. 2008; Zhang et al. 2008). Overexpression of Spindlin1 perturbs the cell cycle, induces chromosome instability, and leads to tumorigenesis (Gao et al. 2005; Yuan et al. 2008; Zhang et al. 2008). In addition, Spindlin1 was shown to function as an activator of Wnt/TCF-4 signaling and promote cancer cell proliferation (Wang et al. 2012). A previous structural study of free Spindlin1 revealed that it consists of three Spin/Ssty motifs organized in a triangular fold, with each Spin/Ssty domain adopting a tudor-like β-barrel fold (Zhao et al. 2007). Recently, Spindlin1 was identified as a histone effector that specifically recognizes H3K4me3; it is enriched in nucleoli of mouse embryonic fibroblast cells during interphase and stimulates the expression of rRNA genes (Wang et al. 2011). In a complementary structural study by the same group, recognition of a H3K4me3 mark by Spindlin1 was shown to involve the second Spin/Ssty motif (Spin/Ssty2) in a recognition mode distinct from other reported H3K4me3 readers (Yang et al. 2012).

Wnt/β-catenin signaling is implicated in a wide range of cellular processes, including proliferation, differentiation, tissue homeostasis, tumorigenesis, apoptosis, and cell survival (Logan and Nusse 2004; Moon et al. 2004; Clevers 2006; MacDonald et al. 2009). Although mechanisms for Wnt signaling regulation are being gradually uncovered, transcriptional regulation of Wnt target genes through histone modification remains unclear. So far, it has been established that Pygopus bound to H3K4me2/3 is essential for Wnt/Wingless signal activation (Fiedler et al. 2008; Gu et al. 2009). Besides, Wnt signaling stimulates histone methyltransferase (HMT) SET8-mediated H4K20me1 to regulate the transcription of a subset of Wnt target genes (Li et al. 2011; Schotta 2011). At the mid-blastula transition (MBT) during *Xenopus* embryonic development, β-catenin stimulates organizer gene transcription by recruiting a histone arginine methyltransferase, PRMT2 (Blythe et al. 2010). Therefore, identification of more "writers," "readers," and "erasers" of histone modification should contribute to a deeper mechanistic understanding of the transcriptional regulation of Wnt target genes.

Here, we report the structural and biophysical characterization of Spindlin1 as a potent histone reader for the dual H3 K4me3–R8me2a methylation pattern. Our subsequent in vivo functional studies revealed that such an activity of histone methylation pattern readout is important for Wnt signaling activation. Spin/Ssty family members have been implicated in multiple roles in health and disease, ranging from early embryogenesis to tumor formation (Staub et al. 2002; Schotta 2011; Wang et al. 2012). Thus, our work provides new insights into Spindlin1 molecular function and paves the way for future progress in Spindlin biology and its therapeutic applications.

Results

Structure of H3K4me3-bound Spindlin1

Using isothermal titration calorimetry (ITC), we measured a dissociation constant (K_d) of ~750 nM between SPIN1$_{50–262}$ (Fig. 1A) and the H3$_{1–20}$K4me3 peptide (Fig. 1B,C). Interestingly, the binding affinity increases approximately fivefold to ~147 nM when a shorter H3$_{1–10}$K4me3 peptide is used (Fig. 1C), suggesting an inhibitory effect of the H3 11–20 segment.

To explore the underlying molecular basis for this recognition, we solved the cocrystal structure of SPIN1$_{50–262}$ bound to the H3$_{1–20}$K4me3 peptide at 1.7 Å resolution (Table 1). Within the H3 1–20 peptide, residues 1–9 could be modeled according to the electron density map (Fig. 1D; Supplemental Fig. S1A). Each Spin/Ssty repeat is composed of four core β strands and one extra β strand, structurally resembling the tudor domain of "Royal Family" family members (Supplemental Fig. S2; Maurer-Stroh et al. 2003). The H3K4me3 mark is inserted into an aromatic cage formed by F141, W151, Y170, and Y177 of Spin/Ssty2, whereby it is stabilized by cation-π and methyl-π interactions (Fig. 1D). The H3-binding surface of Spindlin1 is enriched with negative charges (Fig. 1E), being ideal for basic histone H3 tail interaction.

In the current complex structure, histone H3 "T6–K9" takes on an extended conformation with the R8 side chain pointing toward pocket 1 (Fig. 1E). In contrast, H3 R8 adopts an opposite orientation and is hydrogen-bonded
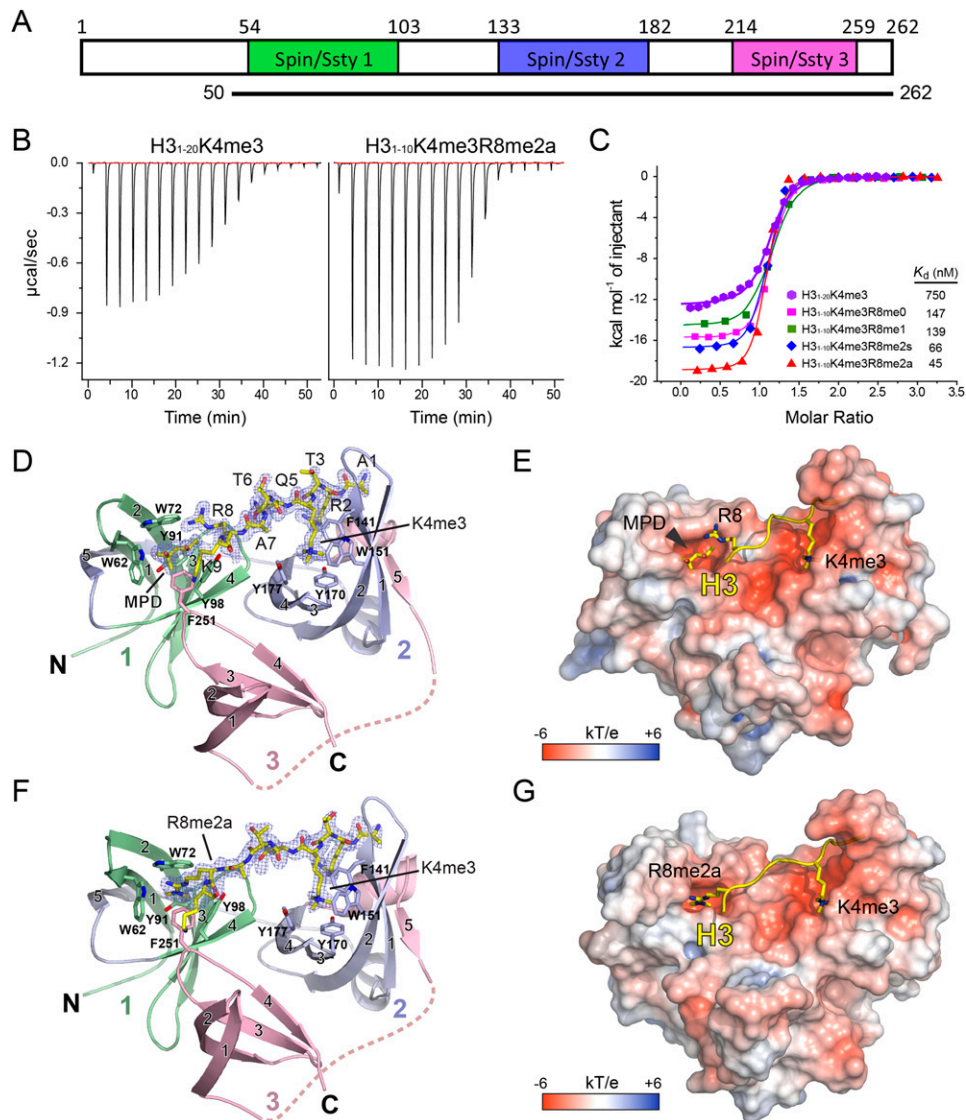
Figure 1. Calorimetric and crystallographic characterization of Spindlin1 as a histone H3 methylation pattern reader. (A) Domain architecture of Spindlin1. The core β-barrel regions of each Spin/Ssty repeat are colored green, blue, and pink, respectively. (Black line) Construct SPIN1$_{50–262}$ used for ITC and structural studies. (B) ITC titration curves of SPIN1$_{50–262}$ with H3$_{1–20}$K4me3 (left) and H3$_{1–10}$K4me3R8me2a (right). (C) ITC fitting curves of SPIN1$_{50–262}$ with histone H3K4me3 peptides of different R8 methylation states. Peptide sequences and complete thermodynamic parameters are listed in Supplemental Table S1. (D,E) Overall structure of SPIN1$_{50–262}$ bound to H3$_{1–20}$K4me3 in ribbon view (D) and electrostatic potential surface view (E). (Blue mesh) 2Fo − Fc omit map contoured at the 1.5 σ level. One molecule of MPD is bound to aromatic pocket 1 of Spin/Ssty. Histone H3 is depicted as yellow sticks. Electrostatic potential is expressed as a spectrum ranging from −6 kT/e (red) to +6 kT/e (blue). Histone peptide was excluded for electrostatic potential calculation. (F,G) Overall structure of SPIN1$_{50–262}$ bound to the dual-mark H3$_{1–10}$K4me3R8me2a peptide, presented in the same way as in D and E. Note the insertion of the asymmetric dimethyl-guanidino group of H3R8 into pocket 1.

to D173 and Y177 of pocket 2 in the structure reported previously (Supplemental Fig. S1B; Yang et al. 2012). Such differences may reflect different crystallization conditions used in the previous and current studies. In support of this, a molecule of 2-methyl-2,4-pentanediol (MPD) from the crystallization buffer was observed within pocket 1 in our structure (Fig. 1D,E), while a molecule of N-cyclohexyl-2-aminoethanesulfonic acid (CHES) was identified within pocket 1 in the previously reported structure (Yang et al. 2012).

The triangular architecture of Spin/Ssty repeats is reminiscent of the triple MBT repeats of L3MBTL1, a lower methyllysine state-specific histone effector (Wang et al. 2003; Li et al. 2007). Despite the triangular shape similarity, Spindlin1 is different from L3MBTL1 in the relative orientation of the triple-module organization. The three Spin/Ssty repeats of Spindlin1 are arranged clockwise, with each repeat facing outward (Supplemental Fig. S3A). In contrast, the three MBT repeats of L3MBTL1 are packed against each other in a face-to-face

Table 1. *Data collection and refinement statistics*

	Spindlin1$_{50-262}$-H3$_{1-20}$K4me3	Spindlin1$_{50-262}$-H3$_{1-10}$K4me3R8me2a	Spindlin1$_{50-262}$-H3$_{1-10}$K4me3R8me2s
Data collection	Native	Native	Native
Space group	P2$_1$	P2$_1$2$_1$2	P2$_1$2$_1$2
Cell dimensions			
a, b, c	122.0 Å, 43.2 Å, 49.8 Å	120.7 Å, 43.3 Å, 50.2 Å	123.0 Å, 41.3 Å, 50.5 Å
α, β, γ	90°, 90°, 90°	90°, 90°, 90°	90°, 90°, 90°
Resolution	50 Å–1.7 Å (1.73 Å–1.70 Å)[a]	50 Å–2.1 Å (2.14 Å–2.10 Å)	50 Å–2.2 Å (2.24 Å–2.20 Å)
R_{sym} or R_{merge}	5.7 (64.5)	9.1 (59.2)	7.2 (61.2)
$I\,I\,\sigma I$	24.8 (2.6)	28.5 (3.7)	21.5 (3.0)
Completeness	99.1% (93.7%)	93.5% (84.0%)	97.3% (91.5%)
Redundancy	4.4 (4.4)	4.6 (4.7)	4.4 (4.3)
Refinement			
Resolution	50 Å–1.7 Å (1.73 Å–1.70 Å)[a]	50 Å–2.1 Å (2.14 Å–2.10 Å)	50 Å–2.2 Å (2.24 Å–2.20 Å)
Number of reflections	245331	68972	58620
R_{work}/R_{free}	18.3/20.7	20.2/25.5	19.6/24.7
Number of atoms			
Protein	3280	1724	1681
Ligand/ion	36	3	1
Water	360	113	75
B-factors			
Protein	29.1	30.3	36.6
Ligand/ion	35.4	30.6	32.9
Water	35.9	33.6	35.8
RMSDs			
Bond lengths	0.007 Å	0.008 Å	0.004 Å
Bond angles	1.17°	1.18°	0.99°

[a]Values in parentheses are for highest-resolution shell.

mode, with the three pockets arranged in an anti-clockwise manner (Supplemental Fig. S3B). Of note, one common feature shared by Spindlin1 and L3MBTL1 is that pocket 2 is used for methylated lysine recognition in both cases.

Structure of Spindlin1 bound to the H3K4me3R8me2a peptide

The fact that H3R8 is positioned in the close vicinity of the aromatic pocket 1 (Fig. 1D,E) prompted us to speculate that methylated H3R8 may be a virtual target for Spindlin1. Intriguingly, the histone H3 modification signature T3ph-K4me3–R8me2a, termed as PMM, has been reported to mark and configure mitotic chromatin in HeLa cells, and an H3 K4me3–R8me2a pattern could be detected as a subepitope of PMM in metaphase chromosomes (Markaki et al. 2009). Given the role of Spindlin1 in cell cycle regulation (Zhao et al. 2007; Yuan et al. 2008; Zhang et al. 2008), it is conceivable that Spindlin1 may function as a signature reader of the H3 K4me3–R8me2a pattern. To test and subsequently confirm our hypothesis, we synthesized H3$_{1-10}$K4me3 peptides with additional R8 modifications containing monomethylation (R8me1), symmetrical dimethylation (R8me2s), and asymmetrical dimethylation (R8me2a) states and performed ITC assays for binding with SPIN1$_{50-262}$. Calorimetric titrations established that SPIN1$_{50-262}$ binds most tightly to H3$_{1-10}$K4me3R8me2a with a K_d of ~45 nM. The binding affinity drops to ~66 nM for H3$_{1-10}$K4me3R8me2s and to ~139 nM for

H3$_{1-10}$K4me3R8me1 (Fig. 1C). Using single R8 methylated peptides, we measured a binding K_d of ~22 μM for the H3$_{1-10}$R8me2a peptide and ~71 μM for the H3$_{1-10}$R8me2s peptide, which is about sevenfold and twofold tighter than the unmodified counterpart ($K_d \approx$ 156 μM) (Supplemental Table S1). Hence, the above results strongly support a role of H3R8 dimethylation in promoting Spindlin1 H3K4me3 recognition.

We next solved the crystal structure of SPIN1$_{50-262}$ in complex with H3$_{1-10}$K4me3R8me2a at 2.1 Å (Table 1). The crystals were grown in an MPD-free condition. In the H3$_{1-10}$K4me3R8me2a complex, we were able to trace H3 residues A1 to K9 in the complex (Fig. 1F; Supplemental Fig. S4A). As anticipated, asymmetrically dimethylated R8 is inserted into pocket 1. There is a snug fit between the asymmetric dimethyl-guanidino group and the aromatic residues (W62, W72, Y91, Y98, and F251) lining pocket 1 (Fig. 1G). Aside from the H3 segment around R8me2a, the new structure of the complex is essentially the same as the H3K4me3 complex, with a superimposition root mean square deviation (RMSD) of 0.33 Å.

In sum, the above ITC and structural studies establish that Spindlin1 is a potent reader of the histone H3 K4me3–R8me2a methylation pattern, in the process engaging its tandem Spin/Ssty repeats 1 and 2 in vitro.

Details of Spindlin1–H3K4me3R8me2a interaction and mutagenesis studies

Recognition of H3K4me3R8me2a peptide by Spindlin1 involves a network of polar interactions in addition to

encapsulation of the two methylation marks by their respective aromatic pockets. As illustrated in Figure 2A, histone H3 segment 1–9 adopts a highly extended conformation, lying across Spin/Ssty repeats 1 and 2. About six sets of water-mediated and eight direct hydrogen bonds or salt bridges were observed between the H3 peptide and Spindlin1 upon complex formation (Fig. 2A, red dashes). Particularly, H3 A1–R2 is anchored in an acidic surface of Spin/Ssty2 through salt bridges between H3A1 α-amine and E142 and D189 as well as between the H3R2 side chain and D184 (Figs. 1G, 2A). The contributions of such salt bridges were validated by binding affinity reductions of approximately threefold for E142A and ~90-fold for D184A (Supplemental Table S1), consistent with mutational studies reported previously (Yang et al. 2012).

The triple Spin/Ssty repeats of Spindlin1 are assembled into a highly integrated globular structure (Fig. 2B). The K4me3 pocket is formed solely by F141, W151, Y170, and Y177 of repeat 2 (Fig. 2B, blue), whereas the R8me2a pocket is formed by W62, W72, and Y91 of repeat 1

(Fig. 2B, green) and F251 of repeat 3 (Fig. 2B, pink). We calculated buried surface areas of 182 Å^2 and 216 Å^2 upon insertion of the trimethylammonium group of K4me3 and the dimethyl-guanidino group of R8me2a, respectively. In addition to the cation-π and methyl-π interactions shared by the two pockets for lysine or arginine methylation readout, R8me2a binding is also facilitated by salt bridge formation with E64 and water-mediated hydrogen-bonding with Y98 (Fig. 2B). To validate the contributions of aromatic caging residues for K4me3 and R8me2a recognition, we performed mutagenesis studies involving these residues. ITC titrations involving a single alanine mutation of aromatic residues F141, Y170, and Y177 resulted in an 80-fold to >800-fold reduction in binding affinity, stressing the importance of an intact K4me3 pocket for efficient binding (Fig. 2C). Likewise, alanine mutation of R8me2a aromatic pocket residues resulted in an approximately threefold binding loss (Supplemental Table S1). Furthermore, an affinity drop of ~10-fold to 40-fold was detected when bulky arginine mutations of residues W72, Y98, and F251 were
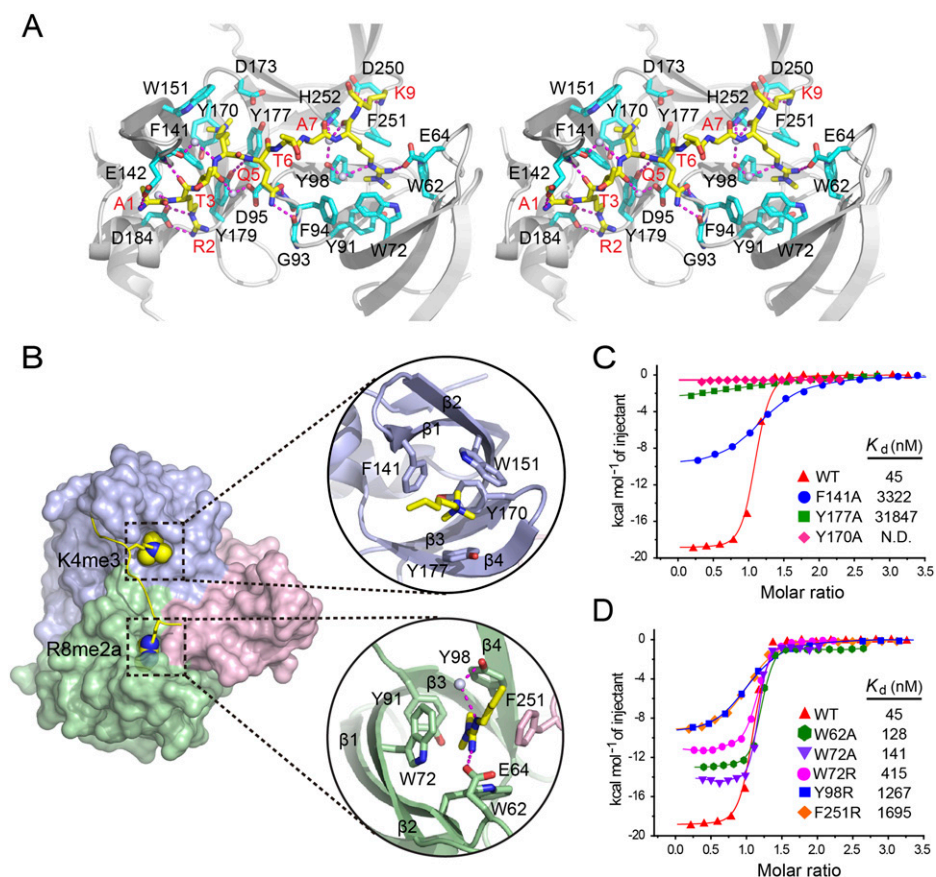
Figure 2. Details of H3 lysine–arginine methylation pattern recognition by Spindlin1 and mutagenesis studies. (*A*) Stereo view of polar contacts between Spindlin1 and the H3K4me3R8me2a peptide. The H3 A1–K9 segment is depicted as yellow sticks. Key Spindlin1 residues involved in histone recognition are colored cyan. (Blue–white balls) Water molecules; (magenta dashes) hydrogen bonds or salt bridges. (*B*) Encapsulation of K4me3 and R8me2a in Spindlin1 pockets 2 and 1. (*Left*) Spindlin1 is shown in surface mode with Spin/Ssty repeats 1, 2, and 3 colored green, blue, and pink, respectively. (*Right*) Close-up views of K4me3 (*top*) and R8me2s (*bottom*) pockets. (*C,D*) ITC fitting curves of Spindlin1 K4me3 (*C*) and R8me2a (*D*) pocket mutants titrated with the H3$_{1–10}$K4me3R8me2a peptide.

introduced (Fig. 2D). Collectively, these results support a role for R8me2a readout in facilitating complex formation.

Asymmetric H3R8 dimethylation state-specific readout by Spindlin1

Arginine may undergo either asymmetrical or symmetrical dimethylation, with the former often linked to gene activation, and the latter linked to repression (Di Lorenzo and Bedford 2011). To explore the molecular basis for arginine methylation state-specific readout, we also solved the cocrystal structure of SPIN1$_{50-262}$ bound to the H3$_{1-10}$K4me3R8me2s peptide at 2.2 Å (Table 1). Despite the same conditions used for crystallization, we failed to observe insertion of R8me2s in pocket 1 under conditions where the electron density for asymmetrical dimethylarginine in the R8me2a complex could be clearly traced (Fig. 3A). In fact, the electron density after H3 Q5 in the R8me2s complex is quite poor (Supplemental Fig. S4B), indicating a loss of stable protein–peptide interactions. Structural alignment studies revealed a conformational adjustment of pocket 1 following the loss of R8me2s insertion (Fig. 3B). In addition to slight side chain rotations of W72, F94, Y98, and F251, the acidic residue E64 notably flips away from a position that allows salt bridge formation with R8me2a (Fig. 3A,B). Collectively, our crystallographic analysis suggests that pocket 1 is not optimal for symmetric dimethylarginine recognition.
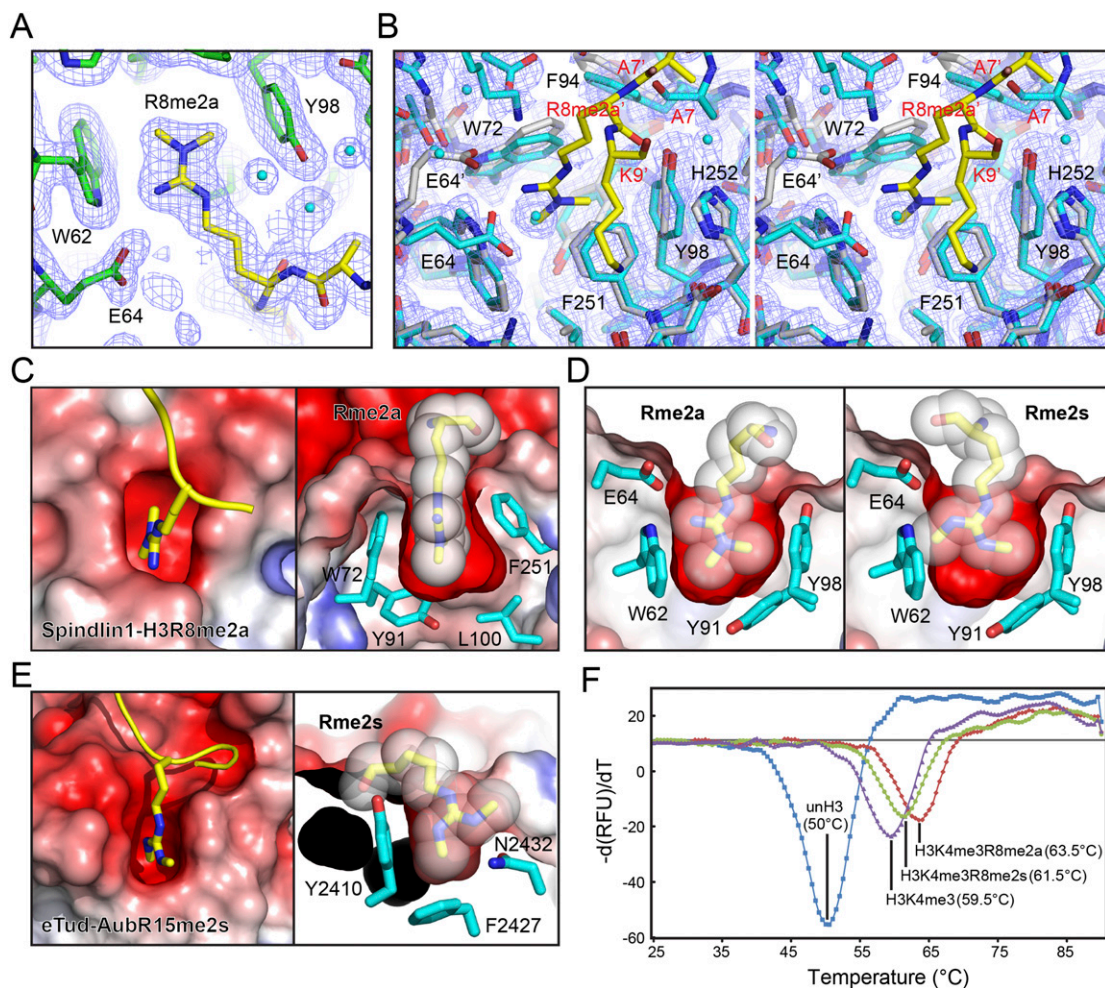
Figure 3. Asymmetric dimethylarginine state-specific recognition by pocket 1 of Spindlin1. (*A*) 2Fo − Fc omit map (one σ level) around pocket 1 in the H3$_{1-10}$K4me3R8me2a complex. (*B*) 2Fo − Fc omit map (one σ level) around pocket 1 in the H3$_{1-10}$K4me3R8me2s complex. The structure of the H3$_{1-10}$K4me3R8me2a complex ([white] protein; [yellow] peptide) was superimposed for comparison. The H3$_{1-10}$K4me3R8me2s complex is colored cyan. R8me2s is invisible due to lack of electron density. Note flipping of the E64 side chain. The figure was prepared in stereo view. (*C,D*) Insertion cavity mode of histone H3 R8me2a recognition by pocket 1 of Spindlin1. (*C*, *left*) Top view. (*Right*) Side cut-away view. (*D*) Front cut-away view. (*Left*) No steric collision upon asymmetrical dimethylarginine (Rme2a) insertion. (*Right*) Steric collision upon symmetrical dimethylarginine (Rme2s) insertion. (*E*) Surface groove mode of Aubergine (Aub) R15me2s recognition by eTud Tudor domain (Protein Data Bank [PDB]: 3NTI). In *C*, *D*, and *E*, protein is shown in an electrostatic surface representation ranging from −6 kT/e (red) to +6 kT/e (blue). (*F*) Thermo-fluor shift melting curves of SPIN1$_{50-262}$ with histone H3 peptides in different methylation states.

A close inspection of pocket 1 in the R8me2a complex reveals an "insertion cavity" mode for Rme2a state-specific recognition (Fig. 3C, left). The dimensions of pocket 1 are relatively deep and narrow, best designed for accommodating the rectangular-shaped asymmetric dimethyl-guanidino group of R8me2a (Fig. 3C [right], D [left]). In contrast, the triangular-shaped symmetric dimethyl-guanidino group of R8me2s is comparatively oversized and may trigger a steric clash upon insertion (modeled in Fig. 3D, right), thereby being unfavorable for pocket 1. Actually, a "surface groove" mode has been reported for Rme2s recognition by several Tudor domains (Chen et al. 2011). One such example is the recognition of Aubergine R15me2s by eTub Tudor (Liu et al. 2010), in which state-specific readout of Rme2s was achieved by an aromatic-lined surface pocket without strict spatial constraints (Fig. 3E). Buried surface analysis revealed a 74.8% ($\sim$182 Å^2) burial of the dimethyl-guanidino group of Rme2s by eTub Tudor, which is in clear contrast with a 90.8% ($\sim$216 Å^2) surface burial in the case of the dimethyl-guanidino group of Rme2a by Spindlin1.

Favorable recognition of H3R8me2a compared with H3R8me2s by Spindlin1 was supported by $\sim$1.5-fold to threefold K_d enhancement and greater heat generation, as revealed in ITC titrations (Supplemental Table S1). In order to evaluate H3R8me2a preference by an independent approach, we also conducted a thermo-fluor stability assay (TSA) of SPIN1$_{50-262}$ mixed with different R8 methylated H3 peptides. Consistent with ITC assays, H3$_{1-10}$K4me3R8me2a displayed the most pronounced stabilization effect. We calculated a melting temperature (Tm) of 63.5°C for H3$_{1-10}$K4me3R8me2a, with the Tm reduced by 2°C for H3$_{1-10}$K4me3R8me2s, by 4°C for H3$_{1-10}$K4me3, and by 13.5°C for unmodified H3$_{1-10}$ (Fig. 3F). It did not escape our attention that symmetrical R8 methylation did enhance H3 peptide binding by Spindlin1 in both ITC and TSA assays. We reasoned that such enhancement may reflect the plasticity of pocket 1 in solution compared with the crystalline state, and such plasticity may render pocket 1 tolerant to R8me2s insertion with a slight preference. Despite this, our crystallographic and solution-based approaches consistently support that Spindlin1 is an H3 Arg8 asymmetric dimethyl state-specific reader.

In vitro H3 K4me3–R8me2a pattern generation by PRMT2 and MLL1 core complex (MLL1c)

The formation of individual histone H3K4me3 and H3R8me2a marks is catalyzed by MLL family proteins (Greer and Shi 2012) and PRMT2 (Blythe et al. 2010; Yang and Bedford 2013), respectively. To explore the biochemical feasibility of establishing an H3 K4me3–R8me2a pattern, we prepared recombinant MLL1c as well as PRMT2 and performed in vitro methylation assays. Using unmodified H3$_{1-21}$ as a substrate, we confirmed the capability of MLL1c and PRMT2 in methylating H3K4 and H3R8 by radiolabeling with [^{3}H]-S-adenosylmethionine ([^{3}H]-SAM) despite the methyltransferase activity of PRMT2 being generally weaker compared with MLL1

(Fig. 4A,B). Next, we synthesized singly modified H3 peptides H3$_{1-21}$R8me2a or H3$_{1-15}$K4me3 and repeated the methylation assay. Although the catalytic efficiency was reduced to $\sim$40%, MLL1c retained considerable H3K4 methyltransferase activity in the presence of a pre-existing H3R8me2a mark (Fig. 4A). Similarly, the existence of H3K4me3 is tolerable for the H3R8 methylation activity of PRMT2 (Fig. 4B). We further performed MALDI-TOF analysis to confirm the production of the H3 H4me3-R8me2a pattern by MLL1c. As expected, a peptide product with a molecular weight of 2679 Da was identified, characteristic of an H3$_{1-21}$ peptide bearing K4me3–R8me2a dual marks (Fig. 4C). The relatively low abundance of the final K4me3 product relative to K4me1 and K4me2 intermediates likely reflects a profile of step-wise methyl group addition catalyzed by MLL1c (Fig. 4C). Collectively, the above in vitro enzymatic assays validate the capability of a K4me3–R8me2a methylation pattern generation by MLL1c as well as by PRMT2.

Spindlin1 directly interacts with TCF4 and prompts Wnt signaling

Although it has been reported that Spindlin1 interacts with TCF4 and promotes cancer cell proliferation through canonical Wnt signaling (Wang et al. 2012), an in-depth molecular mechanism elucidating this pathway remains largely unknown. We first examined whether Spindlin1 could interact with TCF4 in vivo. As expected, Spindlin1 coimmunoprecipitated with TCF4 in HCT116 cells (Fig. 5A). Domain mapping analysis revealed that the Spin/Ssty triple repeats (50–262 amino acids) as well as repeats 1 and 2 (50–193 amino acids) bound to TCF4 strongly, while the N terminus is most likely inhibitory, since full-length Spindlin1 (1–262 amino acids) interacted with TCF4 weakly (Fig. 5B). Using GST-Spin1$_{50-262}$ as bait, we further found that TCF4 interacted with Spindlin1 mainly through its C-terminal domain (401–596 amino acids) (Fig. 5C, left). Since the surface of Spindlin1 repeats 1 and 2 is negatively charged (Fig. 1E), we next searched for arginine/lysine-rich motifs within the TCF4 C-terminal domain with an aim toward identification of a peptide segment potentially responsible for Spindlin1 interaction. Through ITC titration assays using synthetic peptides, we identified such a sequence motif (RRKKKCVRYIQG) spanning residues 458–469 of TCF4. We measured a binding K_d of 3.9 μM between the TCF4$_{458-469}$ peptide and SPIN1$_{50-262}$ (Fig. 5D; Supplemental Table S1). To further confirm that this motif is responsible for Spindlin1/TCF4 interaction, we generated TCF4-C$_{470-596}$ lacking TCF4$_{458-469}$. A GST pull-down assay revealed that this shorter C-terminal segment completely lost its Spindlin1-binding activity (Fig. 5C, right).

Next, we measured Wnt-responsive luciferase reporter activity in HCT116 cells upon Spindlin1 overexpression and observed a dose-dependent potentiation of the Wnt/β-catenin signaling (Fig. 5E), suggesting that Spindlin1 is indeed a positive regulator of the Wnt signaling pathway.
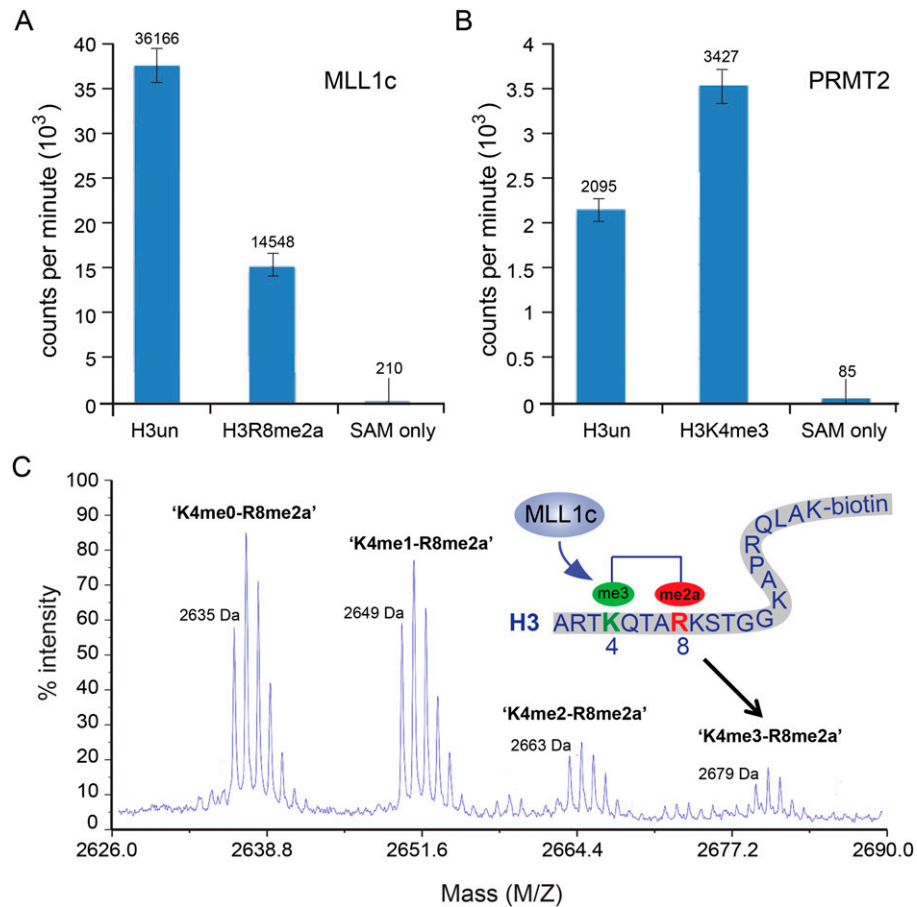
Figure 4. In vitro enzymatic generation of the H3 K4me3–R8me2a pattern by MLL1c and PRMT2. (*A*) HMT activity assay on unmodified (H3un) and R8me2a-modified (H3R8me2a) H3 peptides by MLL1c. Enzymatic activity was monitored by scintillation count of [^{3}H]-labeled H3K4 methylated products. (*B*) HMT activity assay on unmodified (H3un) and K4me3-modified (H3K4me3) peptides by PRMT2. Enzymatic activity was monitored by scintillation count of [^{3}H]-labeled H3R8 methylated products. (*C*) MALDI-TOF mass spectrometry analysis of H3 K4me–R8me2a dual-mark peptide products catalyzed by MLL1c.

To further confirm these results, we silenced endogenous Spindlin1 in HCT116 cells using specific siRNAs and observed reduced Wnt signaling (Fig. 5F). This down-regulation was specific, since it was rescued by over-expression of mouse Spindin1 (Fig. 5F). Moreover, quantitative PCR (qPCR) analysis demonstrated that the mRNA levels of Wnt target genes *CyclinD1*, *Axin2*, *Tiam1*, and *ID-2* were all down-regulated in Spindlin1 knockdown cells (Fig. 5G). Accordingly, the protein levels of Cyclin D1 and Axin2 were both markedly down-regulated (Fig. 5H). Together, these results indicate that Spindlin1 is involved in Wnt signaling activation in colon cancer cells.

Spindlin1 prompts Wnt signaling through its methylation reader activity

Previous studies reported that H3K4me3 plays a key role in transcriptional regulation of Wnt target genes (Willert and Jones 2006; Fiedler et al. 2008). Moreover, β-catenin could recruit PRMT2 to induce H3R8me2a modification in priming organizer gene expression of *Xenopus* embryos

(Blythe et al. 2010). Here we found that Spindlin1 had the capacity to recognize H3K4me3 and H3R8me2a simultaneously. Hence, it is conceivable that Spindlin1 may promote Wnt signaling via recognition of a *cis*-tail H3 K4me3–R8me2a pattern.

To confirm the involvement of PRMT2 in Wnt signaling, we introduced specific siRNA against PRMT2 into HCT116 cells and observed that silencing of PRMT2 could effectively reduce Wnt signaling (Fig. 5I). The qPCR results further confirmed that the expression of Wnt target genes was inhibited (Fig. 5J), and, consistently, their protein levels also dropped (Fig. 5K). These results suggested that PRMT2 is also required for full Wnt signaling in colon cancer cells. Subsequently, we carried out a reporter assay and observed that knockdown of PRMT2 attenuated Spindlin1-promoted Wnt signaling (Fig. 5L), which implied that the transactivation potential of Spindlin1 on Wnt signaling depends on PRMT2, probably through its activity to methylate H3R8. In sum, the above functional studies indicate that Spindlin1 is a positive regulator of Wnt signaling downstream from PRMT2.
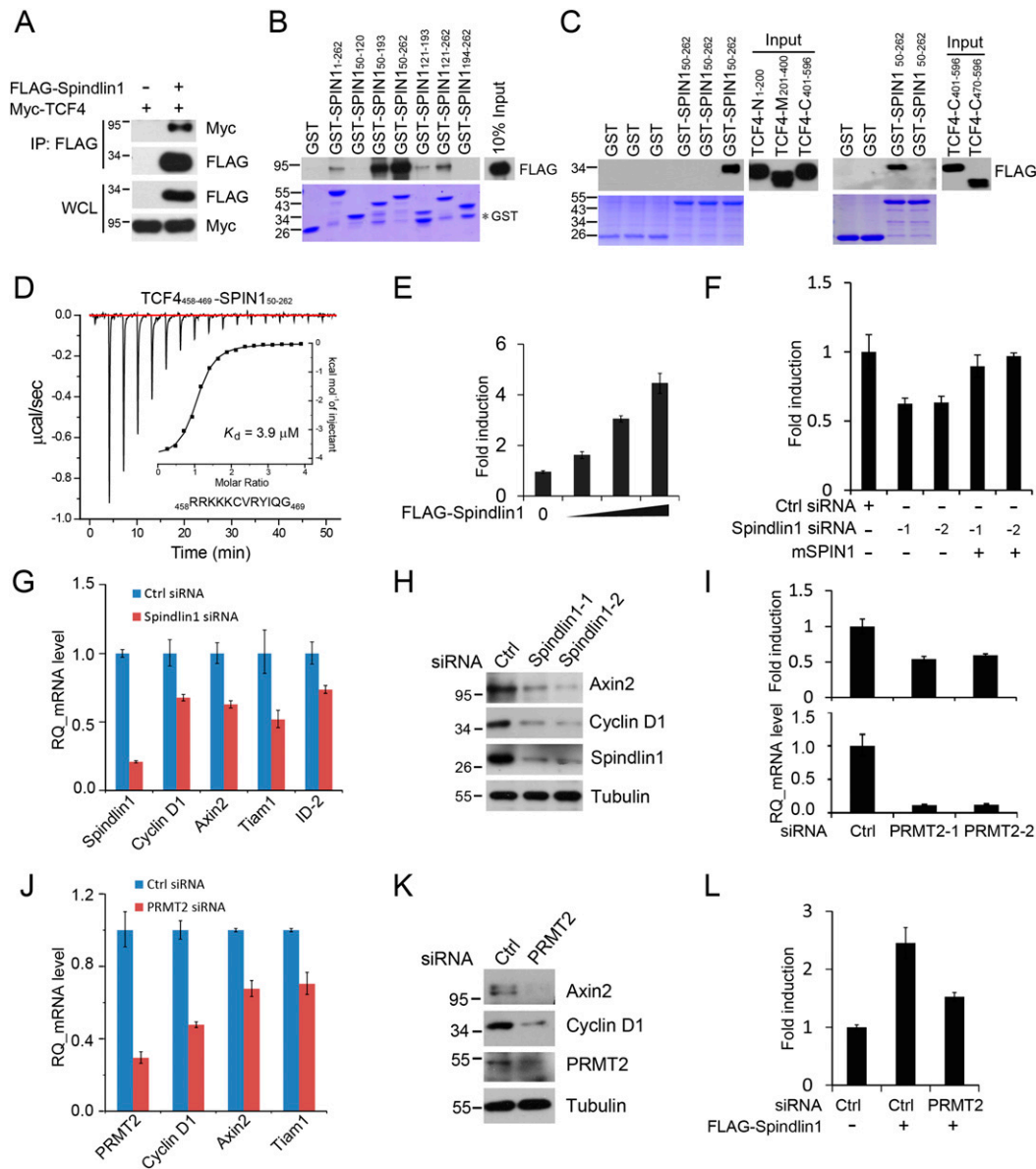
Figure 5. Involvement of Spindlin1 and PRMT2 in Wnt signaling. (*A*) Cell lysates from HCT116 cells transfected with Flag-Spindlin1 and Myc-TCF4 plasmids were subjected to immunoprecipitation (IP) with anti-Flag M2 beads. Whole-cell lysates (WCL) and immunoprecipitates were subjected to immunoblotting with the indicated antibodies. (*B,C*) GST pull-down-based domain mapping between Spindlin1 and TCF4. GST-tagged Spindlin1 fragments were purified from *Escherichia coli*. Flag-tagged full-length TCF4$_{1-596}$, TCF4-N$_{1-200}$, TCF4-M$_{201-400}$, TCF4-C$_{401-596}$, and TCF4-C$_{470-596}$ were immunopurified from HEK293T cells and eluted by Flag peptide. Pull-down bands were detected by immunoblotting with anti-Flag antibody. Purities of the GST-tagged Spindlin1 fragments were verified by Commassie blue staining. (*)Degradation GST band. (*D*) ITC titration and fitting curves of SPIN1$_{50-262}$ with the synthetic TCF4 peptide spanning residues 458–469. (*E*) Wnt-responsive luciferase reporter assays in HCT116 cells transfected with Flag-Spindlin1 in a dose-dependent manner. (*F*) Wnt-responsive luciferase reporter assays in HCT116 cells transfected with control (Ctrl) or two Spindlin1 siRNAs. Where noted, mouse SPIN1 (mSPIN1) was overexpressed. (*G*) Real-time PCR analysis of Wnt target genes in HCT116 cells transfected with control (Ctrl) or Spindlin1 siRNAs. (*H*) Immunoblotting of whole-cell lysates derived from HCT116 cells transfected with control (Ctrl) or Spindlin1 siRNAs. (*I*, *top* panel) Wnt-responsive luciferase reporter assays in HCT116 cells transfected with control (Ctrl) or PRMT2 siRNAs. (*Bottom* panel) Quantification of the knockdown effect was defined by qPCR. (*J*) Real-time qPCR assays of Wnt target genes in HCT116 cells transfected with control (Ctrl) or PRMT2 siRNAs. (*K*) Immunoblotting of whole-cell lysates derived from HCT116 cells transfected with control (Ctrl) or PRMT2 siRNAs. (*L*) Wnt-responsive luciferase reporter assays in HCT116 cells transfected with control (Ctrl) or PRMT2 siRNAs. Where noted, Flag-Spindlin1 was introduced to activate Wnt signaling.

To test the direct involvement of H3K4me3, H3R8me2a, PRMT2, and Spindlin1 in Wnt target gene expression, we performed ChIP (chromatin immunoprecipitation) analysis in HCT116 cells. Consistent with a role in active transcription, promoter regions of *Cyclin D1*, *Axin2*, and *c-myc* were significantly enriched with H3K4me3 modification using an anti-H3K4me3 antibody, while they were not immunoprecipitated by an anti-H3K9me3 antibody (Fig. 6A). More importantly, ChIP using an anti-H3R8me2a antibody revealed that the H3R8me2a modification indeed exists in the same promoter regions of the Wnt target genes (Fig. 6B). In contrast, H3R8me2s was not enriched in the promoters of *Cyclin D1* and *Axin2* but could be clearly detected at the transcriptionally silenced gene locus, such as *β-globin* (Fig. 6C). These results suggest that the promoter regions of Wnt target genes may contain dual modifications of histone H3K4me3 and H3R8me2a.

Of note, the commercially available antibodies developed for single H3K4me3 or H3R8me2a marks were shown to tolerate a dual methylation pattern in our dot blot assays (Supplemental Fig. S5). PRMT2 has been proposed as an H3R8me2a writer on Wnt targets (Blythe et al. 2010); our ChIP results confirmed that the transfected Flag-PRMT2 was bound to the promoters of *Cyclin D1* and *Axin2* in HCT116 cells (Fig. 6D). We also performed ChIP using transiently transfected Flag-Spindlin1 in HCT116 cells. As anticipated, we observed significant enrichment of Spindlin1 at the same promoter regions of multiple Wnt target genes (Fig. 6E).

To further confirm that a histone methylation reader activity is important for Wnt signaling activation by Spindlin1, we introduced "reader pocket"-defective mutants into HCT116 cells to investigate their impact on Wnt target gene expression. We observed that mutations
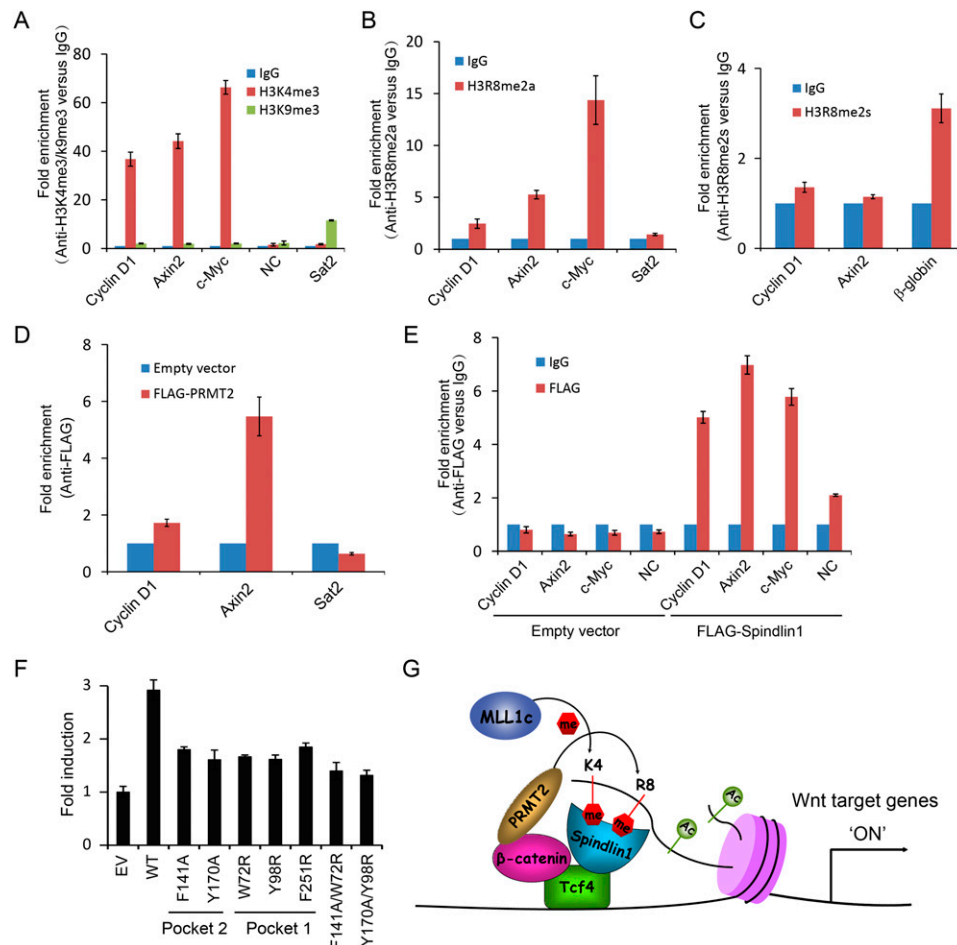
Figure 6. Spindlin1 regulates Wnt signaling through its reader function. (*A–C*) Analysis of H3K4me3 (*A*), H3R8me2a (*B*), and H3R8me2s (*C*) enrichment on the promoter regions of Wnt target genes by ChIP in HCT116 cells. H3K4me3, H3R8me2a, and H3R8me2s enrichment was quantified by qPCR with the indicated primers. NC (negative control) is a negative primer set. Sat2 is a positive primer set for H3K9me3. β-Globin is a positive primer set for H3R8me2s. (*D*) Enrichment of the promoter regions of Wnt target genes with anti-Flag as determined by ChIP in HCT116 cells transfected with Flag-empty vector or Flag-PRMT2. (*E*) Enrichment of the promoter regions of Wnt target genes with anti-Flag or nonspecific IgG as determined by ChIP in HCT116 cells transfected with Flag-empty vector or Flag-Spindlin1. (*F*) Wnt-responsive luciferase reporter assays in HCT116 cells transfected with wild-type Flag-Spindlin1 or its reader pocket point mutants. (EV) Empty vector. (*G*) A schematic model of Spindlin1-regulated Wnt target genes expression.

within either pocket displayed reduced potential to activate Wnt signaling in comparison with wild-type Spindlin1 (Fig. 6F), suggesting an important role of both pockets for Spindlin1 function, most likely through the activity of dual histone H3 methylation pattern readout (Fig. 6G).

Discussion

Histone PTMs and their readout have emerged as a fundamental epigenetic mechanism in regulating many chromatin-templated cellular processes, such as transcription, replication, and mitosis. The fact that histone PTMs often occur in patterns has called attention to the theme of combinatorial readout by paired reader modules in mediating downstream cellular events (Ruthenburg et al. 2007). Recently, chromatin has attracted much attention regarding its emerging role as an information hub or a platform for cellular signal integration and storage (Badeaux and Shi 2013; Johnson and Dent 2013). In this study, we report the structural and functional characterization of Spindlin1 as a unique histone effector that senses an H3 lysine–arginine methylation pattern and participates in Wnt signaling at the transcriptional level.

Our crystal structural analysis established that Spindlin1 uses two aromatic pockets within its tandem Spin/Ssty repeats 1 and 2 for corecognition of H3R8me2a and H3K4me3, respectively. Point mutations of aromatic residues lining either pocket compromised Spindlin1–H3 interaction in vitro and affected Wnt signaling in vivo, suggesting the importance of both pockets. Notably, we measured a binding K_d of 45 nM, which represents the most pronounced binding among reported histone "reader–mark" pairs and stresses the cooperative potential for combinatorial readout. Detailed interaction analysis also pointed to a role of H3 R2 in prompting Spindlin1–H3 interaction through ion pair formation with D184 (Fig. 2A), further adding to the combinatorial complexity. Methylation of lysine and arginine residues has also been implicated in "methyl–methyl" binary switch regulation (Migliori et al. 2010; Di Lorenzo and Bedford 2011). However, here we show that methylated lysine and arginine residues could cooperatively work together to recruit a downstream effector. The way Spindlin1 uses two separate domains for combinatorial lysine–arginine methylation pattern readout is different from available structures, such as PHD fingers from RAG2 (Ramon-Maiques et al. 2007) and Pygopus (Fiedler et al. 2008), double Chromo from CHD1 (Flanagan et al. 2005), and tandem Tudor from Sfg29 (Bian et al. 2011). In the latter cases, a single effector module was shown to involve in H3 R2–K4 methylation pattern recognition with limited cooperativity.

Both K4me3 and R8me2a were recognized using an insertion cavity binding mode (Fig. 2B, left), similar to what has been described for L3MBTL1 (Li et al. 2007). Such a recognition mode usually confers more stringent methylation state specificity due to burial of nearly all methyl groups (Taverna et al. 2007). In support of this, we

observed an ∼10-fold affinity reduction upon loss of one methyl group from H3 K4me3–R8me2a (K_d ≈ 45 nM) to K4me2–R8me2a (K_d ≈ 510 nM) (Supplemental Table S1). In most cases, H3K4me3 was recognized in a "surface groove" mode, and an approximately twofold binding difference was usually observed between trimethylation and dimethylation states; e.g., in the case of the BPTF PHD finger (Li et al. 2007). Likewise, the H3R8me2a pocket is deep and narrow, perfected for encapsulating an asymmetric dimethylarginine group. It is noteworthy that completion of the H3R8me2a pocket requires the contribution of F251 from the third Spin/Ssty repeat, emphasizing the strategy of composite pocket formation for histone mark readout (Iwase et al. 2011; Li and Li 2012; Patel and Wang 2013).

Wnt/β-catenin has been reported to induce H3K4me3, H3R8me2a, and H4K20me1 modifications through MLL1/MLL2, PRMT2 and Set8, respectively (Sierra et al. 2006; Blythe et al. 2010; Li et al. 2011). During frog early embryogenesis, β-catenin could directly recruit PRMT2 and stimulate H3R8me2a to trigger organizer gene expression (Blythe et al. 2010). Consistently, our ChIP assays revealed that PRMT2 and H3R8me2a as well as Spindlin1 and H3K4me3 are all enriched at the promoter regions of Wnt target genes in colon cancer cells (Fig. 6A–E). These results strongly suggest a direct role of Spindlin1, PRMT2, H3K4me3, and H3R8me2a in the expression of Wnt target genes. In support of this, we found that both mRNA and protein levels of Wnt target genes were indeed reduced when Spindlin1 or PRMT2 was down-regulated using siRNAs (Fig. 5F–L). Given the fact that both MLL1 and PRMT2 are capable of generating the H3 K4me3–R8me2a pattern in vitro (Fig. 4A–C), there is a likelihood for homeostasis of such a combinatorial pattern in vivo. As a reader for histone modification in Wnt signaling, Pygopus has been shown to be recruited by BCL9/Legless to physically associate with β-catenin (Gu et al. 2009). Here, we demonstrated that Spindlin1 is another histone effector that has the capacity for recognizing H3K4me3 and H3R8me2a simultaneously and then activates Wnt signaling. Interestingly, Spindlin1 interacts physically with TCF4, notably through an arginine/lysine-rich motif at the C-terminal domain of TCF4 (Fig. 5A–D), suggesting a direct role of Spindlin1 in bridging histone methylation and the β-catenin/TCF4 complex. Taken together, our work establishes a profound linkage among principle Wnt transcription factors (β-catenin/TCF4), epigenetic writers (PRMT2/MLL1c), and a novel histone methylation pattern reader, Spindlin1, which operate synergistically to prompt Wnt signaling at the transcription level (Fig. 6G).

Spindlin1 and its family members have been implicated in early embryogenesis, the cell cycle, gene transcription, and cell signaling. Our work defines Spindlin1 as an important histone methylation pattern reader that integrates a histone-binding activity with multiple cellular pathways. Accumulating evidence supports the concept that miswriting, misinterpretation, and miserasure of histone modifications can contribute to human cancer progression (Chi et al. 2010; Greer and Shi 2012).

Intriguingly, Spindlin1 and PRMT2 are both over-expressed in many human malignant tumors (Wang et al. 2012; Zhong et al. 2012). Given the oncogenic and Wnt-prompting activity of Spindlin1, disruption of the methyl pattern readout of Spindlin1 may open a new avenue for cancer therapeutics (Jiang et al. 2008; Ying and Tao 2009).

Materials and methods

Protein and peptide preparation

Human *Spindlin1* 50–262 (SPIN1$_{50-262}$) was cloned on the pRSFDuet vector with an N-terminal 6xHis tag. Human *MLL1* SET domains, *WDR5*, *RbBP5*, and *Ash2L* were cloned on a pET28a-based vector containing an N-terminal 6xHis-Sumo tag. Human *PRMT2* was cloned on the pGEX-6p2 vector with an N-terminal GST tag. Recombinant proteins were over-expressed in the *Escherichia coli* BL21 (DE3) strain and extensively purified for structural and biochemical studies. Detailed expression and purification procedures are described in the Supplemental Material.

All synthetic histone H3 peptides (>98% purity) were purchased from Scilight Biotechnology LLC.

ITC

Calorimetric experiments were conducted at 25°C with a MicroCal iTC200 instrument (GE Healthcare). The SPIN1$_{50-262}$ samples were dialyzed against the buffer containing 150 mM NaCl and 20 mM HepesNa (pH 7.5). Protein concentration was determined by absorbance spectroscopy at 280 nm. Peptides were quantified by weighing on a large scale. Acquired calorimetric titration data were analyzed using Origin 7.0 (GE Healthcare) using the One Set of Binding Sites fitting model.

TSA

The TSA was performed with a CFX96 real-time PCR instrument (Bio-Rad). A typical TSA solution is composed of 0.4 mg/mL SPIN1$_{50-262}$, 1× Sypro Orange (Invitrogen), and 40 μM histone peptide. All solutions were prepared in 25 μL under the same buffer (150 mM NaCl, 20 mM HepesNa at pH 7.5), with the identity of histone peptide being the sole variable. During TSA assays, all samples were heated from 25°C to 90°C at a rate of 0.5°C per minute. Protein denaturation was monitored by increased fluorescence signal of Sypro Orange, which captures exposed hydrophobic residues during thermal unfolding. The recorded curves were analyzed by the software CFX-Manager (Bio-Rad). The temperature corresponding to the inflection point was defined as Tm.

X-ray crystallographic studies

All crystals were grown by the sitting-drop vapor diffusion method at 18°C. Drops were prepared by mixing 1 μL of protein complex with 1 μL of reservoir solution. Detailed crystallization conditions are listed in the Supplemental Material.

Crystals were flash-frozen in liquid nitrogen under cryoprotectant conditions (reservoir solution supplemented with 12% glycerol). Diffraction data were collected at beamline BL17U of the Shanghai Synchrotron Radiation Facility. All data sets were indexed and merged using the HKL2000 suite (Otwinowski and Minor 1997). Data processing statistics are summarized in Table 1. Crystal structures were determined by molecular replacement using MOLREP (Vagin and Teplyakov 2010) with free Spindlin1 (Protein Data Bank [PDB] 2NS2) as a search model. Model building and refinement were performed with COOT (Emsley and Cowtan 2004) and PHENIX (Adams et al. 2010), respectively. The refined structures were validated by Procheck (Laskowski et al. 1993). Ramachandran plot analysis showed that all residues of the three complex structures are within the most favored or allowed regions. Detailed structural refinement statistics are summarized in Table 1.

Structural analysis and figure preparation were mostly done using the program PyMol version 1.6 (http://www.pymol.org). Electrostatic potential surfaces were calculated by the APBS tool (Baker et al. 2001) in PyMol version 1.6. Simulated annealing omit maps were generated by PHENIX (Adams et al. 2010). Buried surface analysis was performed with PDBePISA (Krissinel and Henrick 2007).

In vitro HMT assays

For MLL family methyltransferases, 25 μM complexes were used for all assays. MLL1 core complexes were assembled in buffer comprising 25 mM Tris (pH 8.0), 150 mM NaCl, and 10% glycerol by combining all components in equal molar ratio. HMT reaction was carried out in the presence of 5 mM SAM and 50 μM H3$_{1-21}$ unmodified or H3$_{1-21}$R8me2a peptides (both peptides were synthesized with additional C-terminal lysine–biotin modification). The mixture was incubated for 1 h at 30°C and diluted 10 times in Millipore water for MALDI-TOF mass spectrometry. For scintillation counting, similar reactions were also performed in the presence of 2.5 mM [^{3}H]-SAM; 5 μL from each enzyme–substrate combination was blotted on P8 filter paper and subsequently washed with 50 mM NaHCO$_3$. Methylation was detected by liquid scintillation in triplicate.

For PRMT2, 20 μg of GST-PRMT2 (bound on resin) was incubated in the presence of 2.5 mM [^{3}H]-SAM with either 50 μM H3$_{1-21}$ unmodified or H3$_{1-15}$K4me3 peptides (both peptides contain additional C-terminal lysine–biotin modification). The reactions were carried out for 8 h at 37°C. After spinning down the resin, 5 μL of each combination was blotted on P8 filter paper and washed with 50 mM NaHCO$_3$. Methylation was detected by liquid scintillation done in triplicate.

GST pull-down assays

Purified Flag-tagged TCF4 and its truncated forms from HEK293T cells were incubated with Glutathione Sepharose 4B beads (GE Healthcare) saturated with bacterially expressed full-length or truncated GST-Spindlin1 overnight at 4°C. The beads were washed four times with histone-binding buffer (50 mM Tris-Cl at pH 7.4, 200 mM NaCl, 0.2% Triton, 10% glycerol, 1 mM EDTA, 1 mM DTT, supplemented with protease inhibitor cocktail [Roche]). The pull-down samples were analyzed by immunoblotting.

Cell culture and plasmids

HCT116 and HEK293T cells were cultured in McCoy's 5A and DMEM, respectively, with 10% fetal bovine serum (FBS) and maintained at 37°C and 5% CO$_2$ atmosphere. All culture media were supplemented with penicillin and streptomycin.

Flag-Spindlin1, Flag-TCF4, and TCF4 truncated forms were generated by subcloning human Spindlin1 and TCF4 cDNAs into the pcDNA3.1-Flag expression vector. Myc-TCF4 was cloned by subcloning human TCF4 into the pcDNA3.1-Myc vector. Mouse Spindlin1 was amplified from mouse cDNA and

subcloned into the pcDNA3.1-Flag vector. Mutations in full-length Spindlin1 (F141A, Y170A, W72R, Y98R, F251R, F141A/W72R, and Y170A/Y98R) were generated by site-directed mutagenesis and confirmed by DNA sequencing.

Luciferase reporter assay

Wnt-responsive luciferase reporter assays in HCT116 cells were carried out in 96-well plates in triplicate as described previously (Zhu et al. 2012). The DNA samples transfected per well were 15 ng of TOPFLASH, 0.5 ng of Renilla, and 50 ng of Spindlin1 and its point mutants.

Immunoblotting and coimmunoprecipitation assay

For immunoblotting, cells were lysed with RIPA buffer (50 mM Tris-Cl at pH 7.4, 150 mM NaCl, 1% NP40, 0.2% SDS, 1 mM DTT, supplemented with protease inhibitor cocktail, 2 mM Na_3VO_4, 25 mM NaF) and sonicated at 20% amplitude for 30 sec (3 sec on, 3 sec off) at 4°C. Cell lysates were resolved by SDS-PAGE after measuring protein concentration by BCA protein assays (Pierce). For coimmunoprecipitation, HEK293T and HCT116 cells transfected with the indicated plasmids were lysed with lysis buffer (50 mM Tris-HCl at pH 7.5, 0.5% Triton, 150 mM NaCl, supplemented with protease inhibitor cocktail [Roche], 2 mM Na_3VO_4, 25 mM NaF) and sonicated at 20% amplitude for 30 sec (3 sec on, 3 sec off) at 4°C. Cell lysates were immunoprecipitated with anti-Flag M2 agarose beads, and the immuno-complexes were washed four times with lysis buffer and subjected to SDS-PAGE and immunoblotting.

RNA extraction, reverse transcription, and real-time PCR

Total RNA extraction was performed with EZ-10 DNAaway RNA miniprep kit (BS88133, Sangon Biotech). Reverse transcription was performed with the Reverse Transcription System (Promega). The ChIP-enriched DNA fragment and Wnt target gene transcription were analyzed by real-time PCR. The reactions were run on an ABI StepOne Plus instrument (Life Technologies). The thermal cycling conditions were 2 min at 96°C followed by 40 cycles of 5 sec at 96°C, 10 sec at 57°C, and 25 sec at 72°C.

ChIP

HCT116 cells were seeded in 10-cm dishes or transfected with DNA plasmids. A final concentration of 1% formaldehyde was added and incubated with gentle rotation for 10 min at room temperature to cross-link DNA–proteins. The cross-linking was terminated by adding 125 mM glycine into the medium and shaking for 5 min. The cells were rinsed with cold PBS twice and then collected. The cells were spun down and rinsed with cold PBS. The pellets were resuspended in 400 µL of SDS lysis buffer (50 mM Tris-Cl at pH 8.1, 10 mM EDTA, 1% SDS, protease inhibitor cocktail [Roche]) in 1.5-mL Eppendorf tubes. Cells were sonicated for six cycles for 6 sec each on ice (27W) with 20 sec on ice between cycles and then centrifuged at 14,000 rpm for 20 min at 4°C. A small aliquot (20 µL) of the supernatant was saved as an input control. The rest of the supernatant (200 µL) was transferred to 2-mL Eppendorf tubes and diluted 10-fold in ChIP dilution buffer (16.7 mM Tris-Cl at pH 8.1, 167 mM NaCl, 1.2 mM EDTA, 1.1% Triton X-100, protease inhibitor). Protein A/G agarose/salmon sperm DNA (50 µL) was added to the tubes and rotated at 4°C to preclear the mixtures. The supernatant was spun down and transferred into new tubes. Antibodies (2 µg of IgG or specific antibodies) were added into the tubes and rotated

overnight at 4°C. On the second day, Protein A/G agarose/salmon sperm DNA (40 µL) were added and rotated for 3 h. The beads were first washed once with low-salt wash buffer (20 mM Tris-HCl at pH 8.1, 150 mM NaCl, 1 mM EDTA, 0.1% SDS, 1% Triton-X100, 0.1% Na-deoxycholate), high-salt immunoprecipitation wash buffer (20 mM Tris-HCl at pH 8.1, 500 mM NaCl, 1 mM EDTA, 0.1% SDS, 1% Triton-X100, 0.1% Na-deoxycholate), and LiCl immunoprecipitation wash buffer (10 mM Tris-HCl at pH 8.1, 250 mM LiCl, 1 mM EDTA, 0.5% NP-40, 0.5% deoxycholic acid) and twice with TE buffer (10 mM Tris-HCl at pH 8.1, 1 mM EDTA). The beads were eluted two times with elution buffer (200 µL of 1% SDS, 10 mM Tris-HCl at pH 8.1, 1 mM EDTA). The samples were incubated overnight at 65°C to reverse the cross-linkage. The DNA was purified and analyzed by real-time PCR. Primer information used for assays is summarized in Supplemental Table S2. Triplicates were performed for each reaction condition.

Accession codes

The atomic coordinates and structure factors for human Spindlin1$_{50–262}$ complexes have been deposited into PDB under accession codes 4MZG for the H3$_{1–20}$K4me3 complex, 4MZF for the H3$_{1–10}$K4me3R8me2a complex, and 4MZH for the H3$_{1–10}$K4me3R8me2s complex.

References

Adams PD, Afonine PV, Bunkoczi G, Chen VB, Davis IW, Echols N, Headd JJ, Hung LW, Kapral GJ, Grosse-Kunstleve RW, et al. 2010. PHENIX: A comprehensive Python-based system for macromolecular structure solution. *Acta Crystallogr D Biol Crystallogr* **66:** 213–221.

Badeaux AI, Shi Y. 2013. Emerging roles for chromatin as a signal integration and storage platform. *Nat Rev Mol Cell Biol* **14:** 211–224.

Baker NA, Sept D, Joseph S, Holst MJ, McCammon JA. 2001. Electrostatics of nanosystems: Application to microtubules and the ribosome. *Proc Natl Acad Sci* **98:** 10037–10041.

Bian C, Xu C, Ruan J, Lee KK, Burke TL, Tempel W, Barsyte D, Li J, Wu M, Zhou BO, et al. 2011. Sgf29 binds histone H3K4me2/3 and is required for SAGA complex recruitment and histone H3 acetylation. *EMBO J* **30:** 2829–2842.

Blythe SA, Cha SW, Tadjuidje E, Heasman J, Klein PS. 2010. β-Catenin primes organizer gene expression by recruiting a histone H3 arginine 8 methyltransferase, Prmt2. *Dev Cell* **19:** 220–231.

Chen C, Nott TJ, Jin J, Pawson T. 2011. Deciphering arginine methylation: Tudor tells the tale. *Nat Rev Mol Cell Biol* **12:** 629–642.

Chi P, Allis CD, Wang GG. 2010. Covalent histone modifications–miswritten, misinterpreted and mis-erased in human cancers. *Nat Rev Cancer* **10:** 457–469.

Clevers H. 2006. Wnt/β-catenin signaling in development and disease. *Cell* **127:** 469–480.

Di Lorenzo A, Bedford MT. 2011. Histone arginine methylation. *FEBS Lett* **585:** 2024–2031.

Emsley P, Cowtan K. 2004. Coot: Model-building tools for molecular graphics. *Acta Crystallogr D Biol Crystallogr* **60:** 2126–2132.

Fiedler M, Sánchez-Barrena MJ, Nekrasov M, Mieszczanek J, Rybin V, Müller J, Evans P, Bienz M. 2008. Decoding of methylated histone H3 tail by the Pygo-BCL9 Wnt signaling complex. *Mol Cell* **30:** 507–518.

Flanagan JF, Mi LZ, Chruszcz M, Cymborowski M, Clines KL, Kim Y, Minor W, Rastinejad F, Khorasanizadeh S. 2005. Double chromodomains cooperate to recognize the methylated histone H3 tail. *Nature* **438:** 1181–1185.

Gao Y, Yue W, Zhang P, Li L, Xie X, Yuan H, Chen L, Liu D, Yan F, Pei X. 2005. Spindlin1, a novel nuclear protein with a role in the transformation of NIH3T3 cells. *Biochem Biophys Res Commun* **335:** 343–350.

Greer EL, Shi Y. 2012. Histone methylation: A dynamic mark in health, disease and inheritance. *Nat Rev Genet* **13:** 343–357.

Gu B, Sun P, Yuan Y, Moraes RC, Li A, Teng A, Agrawal A, Rheaume C, Bilanchone V, Veltmaat JM, et al. 2009. Pygo2 expands mammary progenitor cells by facilitating histone H3 K4 methylation. *J Cell Biol* **185:** 811–826.

Iwase S, Xiang B, Ghosh S, Ren T, Lewis PW, Cochrane JC, Allis CD, Picketts DJ, Patel DJ, Li H, et al. 2011. ATRX ADD domain links an atypical histone methylation recognition mechanism to human mental-retardation syndrome. *Nat Struct Mol Biol* **18:** 769–776.

Jenuwein T, Allis CD. 2001. Translating the histone code. *Science* **293:** 1074–1080.

Jiang X, Tan J, Li J, Kivimae S, Yang X, Zhuang L, Lee PL, Chan MT, Stanton LW, Liu ET, et al. 2008. DACT3 is an epigenetic regulator of Wnt/β-catenin signaling in colorectal cancer and is a therapeutic target of histone modifications. *Cancer Cell* **13:** 529–541.

Johnson DG, Dent SY. 2013. Chromatin: Receiver and quarterback for cellular signals. *Cell* **152:** 685–689.

Krissinel E, Henrick K. 2007. Inference of macromolecular assemblies from crystalline state. *J Mol Biol* **372:** 774–797.

Laskowski RA, Moss DS, Thornton JM. 1993. Main-chain bond lengths and bond angles in protein structures. *J Mol Biol* **231:** 1049–1067.

Li Y, Li H. 2012. Many keys to push: Diversifying the 'readership' of plant homeodomain fingers. *Acta Biochim Biophys Sin (Shanghai)* **44:** 28–39.

Li H, Fischle W, Wang W, Duncan EM, Liang L, Murakami-Ishibe S, Allis CD, Patel DJ. 2007. Structural basis for lower lysine methylation state-specific readout by MBT repeats of L3MBTL1 and an engineered PHD finger. *Mol Cell* **28:** 677–691.

Li Z, Nie F, Wang S, Li L. 2011. Histone H4 Lys 20 monomethylation by histone methylase SET8 mediates Wnt target gene activation. *Proc Natl Acad Sci* **108:** 3116–3123.

Liu H, Wang JY, Huang Y, Li Z, Gong W, Lehmann R, Xu RM. 2010. Structural basis for methylarginine-dependent recognition of Aubergine by Tudor. *Genes Dev* **24:** 1876–1881.

Liu K, Guo Y, Liu H, Bian C, Lam R, Liu Y, Mackenzie F, Rojas LA, Reinberg D, Bedford MT, et al. 2012. Crystal structure of TDRD3 and methyl-arginine binding characterization of TDRD3, SMN and SPF30. *PLoS ONE* **7:** e30375.

Logan CY, Nusse R. 2004. The Wnt signaling pathway in development and disease. *Annu Rev Cell Dev Biol* **20:** 781–810.

MacDonald BT, Tamai K, He X. 2009. Wnt/β-catenin signaling: Components, mechanisms, and diseases. *Dev Cell* **17:** 9–26.

Markaki Y, Christogianni A, Politou AS, Georgatos SD. 2009. Phosphorylation of histone H3 at Thr3 is part of a combinatorial pattern that marks and configures mitotic chromatin. *J Cell Sci* **122:** 2809–2819.

Maurer-Stroh S, Dickens NJ, Hughes-Davies L, Kouzarides T, Eisenhaber F, Ponting CP. 2003. The Tudor domain 'Royal Family': Tudor, plant Agenet, Chromo, PWWP and MBT domains. *Trends Biochem Sci* **28:** 69–74.

Migliori V, Phalke S, Bezzi M, Guccione E. 2010. Arginine/lysine-methyl/methyl switches: Biochemical role of histone arginine methylation in transcriptional regulation. *Epigenomics* **2:** 119–137.

Migliori V, Muller J, Phalke S, Low D, Bezzi M, Mok WC, Sahu SK, Gunaratne J, Capasso P, Bassi C, et al. 2012. Symmetric dimethylation of H3R2 is a newly identified histone mark that supports euchromatin maintenance. *Nat Struct Mol Biol* **19:** 136–144.

Moon RT, Kohn AD, De Ferrari GV, Kaykas A. 2004. WNT and β-catenin signalling: Diseases and therapies. *Nat Rev Genet* **5:** 691–701.

Musselman CA, Lalonde ME, Cote J, Kutateladze TG. 2012. Perceiving the epigenetic landscape through histone readers. *Nat Struct Mol Biol* **19:** 1218–1227.

Oh B, Hwang SY, Solter D, Knowles BB. 1997. Spindlin, a major maternal transcript expressed in the mouse during the transition from oocyte to embryo. *Development* **124:** 493–503.

Otwinowski Z, Minor W. 1997. Processing of X-ray diffraction data collected in oscillation mode. In *Methods in enzymology: Macromolecular crystallography, part A* (ed. Carter CW Jr, Sweet RM), Vol. 276, pp. 307–326. Academic Press, New York.

Patel DJ, Wang Z. 2013. Readout of epigenetic modifications. *Annu Rev Biochem* **82:** 81–118.

Ramon-Maiques S, Kuo AJ, Carney D, Matthews AG, Oettinger MA, Gozani O, Yang W. 2007. The plant homeodomain finger of RAG2 recognizes histone H3 methylated at both lysine-4 and arginine-2. *Proc Natl Acad Sci* **104:** 18993–18998.

Ruthenburg AJ, Li H, Patel DJ, Allis CD. 2007. Multivalent engagement of chromatin modifications by linked binding modules. *Nat Rev Mol Cell Biol* **8:** 983–994.

Schotta G. 2011. H4K20 monomethylation faces the WNT. *Proc Natl Acad Sci* **108:** 3097–3098.

Sierra J, Yoshida T, Joazeiro CA, Jones KA. 2006. The APC tumor suppressor counteracts β-catenin activation and H3K4 methylation at Wnt target genes. *Genes Dev* **20:** 586–600.

Sikorsky T, Hobor F, Krizanova E, Pasulka J, Kubicek K, Stefl R. 2012. Recognition of asymmetrically dimethylated arginine by TDRD3. *Nucleic Acids Res* **40:** 11748–11755.

Staub E, Mennerich D, Rosenthal A. 2002. The Spin/Ssty repeat: A new motif identified in proteins involved in vertebrate development from gamete to embryo. *Genome Biol* **3:** RESEARCH0003.

Taverna SD, Li H, Ruthenburg AJ, Allis CD, Patel DJ. 2007. How chromatin-binding modules interpret histone modifications: Lessons from professional pocket pickers. *Nat Struct Mol Biol* **14:** 1025–1040.

Vagin A, Teplyakov A. 2010. Molecular replacement with MOLREP. *Acta Crystallogr D Biol Crystallogr* **66:** 22–25.

Wang Z, Patel DJ. 2011. Combinatorial readout of dual histone modifications by paired chromatin-associated modules. *J Biol Chem* **286:** 18363–18368.

Wang WK, Tereshko V, Boccuni P, MacGrogan D, Nimer SD, Patel DJ. 2003. Malignant brain tumor repeats: A three-

leaved propeller architecture with ligand/peptide binding pockets. *Structure* **11:** 775–789.

Wang W, Chen Z, Mao Z, Zhang H, Ding X, Chen S, Zhang X, Xu R, Zhu B. 2011. Nucleolar protein Spindlin1 recognizes H3K4 methylation and stimulates the expression of rRNA genes. *EMBO Rep* **12:** 1160–1166.

Wang JX, Zeng Q, Chen L, Du JC, Yan XL, Yuan HF, Zhai C, Zhou JN, Jia YL, Yue W, et al. 2012. SPINDLIN1 promotes cancer cell proliferation through activation of WNT/TCF-4 signaling.*Mol Cancer Res* **10:** 326–335.

Willert K, Jones KA. 2006. Wnt signaling: Is the party in the nucleus?. *Genes Dev* **20:** 1394–1404.

Yang Y, Bedford MT. 2013. Protein arginine methyltransferases and cancer. *Nat Rev Cancer* **13:** 37–50.

Yang Y, Lu Y, Espejo A, Wu J, Xu W, Liang S, Bedford MT. 2010. TDRD3 is an effector molecule for arginine-methylated histone marks. *Mol Cell* **40:** 1016–1023.

Yang N, Wang W, Wang Y, Wang M, Zhao Q, Rao Z, Zhu B, Xu RM. 2012. Distinct mode of methylated lysine-4 of histone H3 recognition by tandem tudor-like domains of Spindlin1. *Proc Natl Acad Sci* **109:** 17954–17959.

Ying Y, Tao Q. 2009. Epigenetic disruption of the WNT/β-catenin signaling pathway in human cancers. *Epigenetics* **4:** 307–312.

Yuan H, Zhang P, Qin L, Chen L, Shi S, Lu Y, Yan F, Bai C, Nan X, Liu D, et al. 2008. Overexpression of SPINDLIN1 induces cellular senescence, multinucleation and apoptosis. *Gene* **410:** 67–74.

Zhang P, Cong B, Yuan H, Chen L, Lv Y, Bai C, Nan X, Shi S, Yue W, Pei X. 2008. Overexpression of spindlin1 induces metaphase arrest and chromosomal instability. *J Cell Physiol* **217:** 400–408.

Zhao Q, Qin L, Jiang F, Wu B, Yue W, Xu F, Rong Z, Yuan H, Xie X, Gao Y, et al. 2007. Structure of human spindlin1. Tandem tudor-like domains for cell cycle regulation. *J Biol Chem* **282:** 647–656.

Zhong J, Cao RX, Zu XY, Hong T, Yang J, Liu L, Xiao XH, Ding WJ, Zhao Q, Liu JH, et al. 2012. Identification and characterization of novel spliced variants of PRMT2 in breast carcinoma. *FEBS J* **279:** 316–335.

Zhu G, Wang Y, Huang B, Liang J, Ding Y, Xu A, Wu W. 2012. A Rac1/PAK1 cascade controls β-catenin activation in colon cancer cells. *Oncogene* **31:** 1001–1012.